ELSEVIER

Journal of Nuclear Materials 300 (2002) 27–38

journal of nuclear materials

www.elsevier.com/locate/jnucmat

Analysis of the monoclinic–tetragonal phase transition of zirconia under irradiation

D. Simeone [a,*], D. Gosset [a], J.L. Bechade [b], A. Chevarier [c]

[a] *Laboratoire de Métallurgie et d'Etude de l'Endommagement, SEMI, CEA, CE Saclay, F-91191 Gif-sur-Yvette cedex, France*
[b] *SRMA, CEA, CE Saclay, F-91191 Gif-sur-Yvette cedex, France*
[c] *IPNL, IN2P3, F-69100 Villeurbanne cedex, France*

Received 7 June 2001; accepted 30 September 2001

Abstract

Zirconia produced by the oxidation of zirconium alloys in nuclear reactors exhibits a phase transition under ionic irradiation, simulating a neutron irradiation. To understand the mechanism responsible for this irradiation driven phase transition, different kinds of projectiles were used to irradiate pure monoclinic zirconia samples. The evolution of these irradiated samples as a function of dpa has been studied using grazing X-ray diffraction. The Rietveld method has been applied on collected X-ray diffraction diagrams to study the phase produced under irradiation and the kinetics of its formation. Even at high dpa values, only the monoclinic and tetragonal phases were used to simulate X-ray diffraction diagrams. No amorphisation of zirconia was observed. The evolution of unit cells and short range strains in both phases under irradiation leads us to think that the irradiation driven transition is martensitic. Supposing that the inelastic stopping power in sub-cascades is responsible for the irradiation driven phase transition, we propose a model based on the Landau–Ginzburg effective hamiltonian to explain both the $m \rightarrow t$ transition observed under irradiation and the $t \rightarrow m$ transition measured during isochronal annealing after irradiation.

1. Introduction

Zirconium alloys are used as cladding elements in nuclear plants because of the low absorption cross-section of zirconium. In Pressurised Water Reactors, the oxidation of these cladding elements leads to the apparition of a zirconia, ZrO_2, layer. This oxide layer drastically modifies the mechanical and thermal behaviour of cladding elements. The noticeable modification of mechanical properties of cladding elements drastically diminishes the lifetime of the nuclear core. To increase the lifetime of the core elements, the behaviour of zirconia under irradiation must be studied with great attention [1].

In non-irradiated zirconia, the monoclinic–tetragonal ($m \rightarrow t$) phase transition is associated to a clear group–subgroup relation [2] and occurs near 1400 K in the temperature–pressure phase diagram [3]. The displacive character of the transition may be produced by a condensation of two phonons at point M of the Brillouin zone of the tetragonal phase ($P4_2/nmc$) of ZrO_2. This $m \rightarrow t$ transition is clearly first order. A discontinuous jump of the unit cell volume is observed at the critical temperature [4]. During this transition, the coordinence of the zirconium cation varies from 8 in the tetragonal phase to 7 in the monoclinic phase. The oxygen polyhedron, a deformed cube embedding the Zr cation (cf. Fig. 1(a)) in the tetragonal phase, distorts to form a pyramid and a tetrahedron in the monoclinic phase (cf. Fig. 1(b)). The Zirconium cation lies at the common

* Corresponding author. Tel.: +33-1 69 08 29 20; fax: +33-1 69 08 90 82.
E-mail address: david.simeone@cea.fr (D. Simeone).

0022-3115/02/$ - see front matter
PII: S0022-3115(01)00701-2

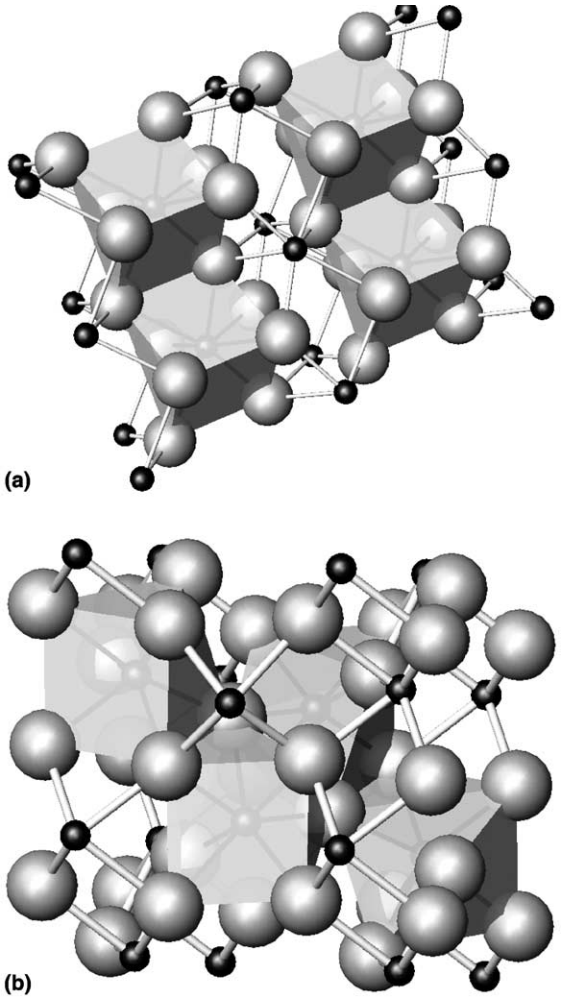

Fig. 1. Description of the tetragonal and monoclinic ZrO_2 unit cells. The 8 bonds between Zr and O atoms are plotted in the coordinence polyhedra (a). During the $m \rightarrow t$ phase transition, this polyhedron is deformed. In the monoclinic phase, the polyhedron is composed of 7 bonds. Caption: large atoms are oxygen atoms; small atoms are zirconium atoms.

vertex of these two polyhedra. During this reconstruction of the oxygen polyhedra in the monoclinic phase, one oxygen atom moves away. The large shift of this oxygen atom does not allow a clear analysis of this transition in terms of Landau free energy formalism, although some attempts were done to analyse the first-order transition as an extension of the Landau theory [5].

In a previous paper [1], we proved that a monoclinic $\rightarrow$ tetragonal ($m \rightarrow t$) phase transition occurs during irradiation at room temperature in a pure monoclinic zirconia. This work extends previous studies on zirconia behaviour under irradiation. The aim of this paper is, on the one hand, to confirm previous investigations on the phase transition of zirconia under irradiation, and on the other hand, to present a possible model to describe effects of irradiation of zirconia.

- Four different kinds of irradiations using 1 MeV electrons, 400 keV O, 800 keV Bi and 400 keV Xe ions at high fluences were performed to analyse the kinetics of the $m \rightarrow t$ phase transition in terms of defect production. The overall kinetics of the $m \rightarrow t$ phase transition is followed using grazing X-ray diffraction. In order to obtain the maximum information on diffraction diagrams, the Rietveld method has been improved to take into account specific errors, especially the angular shift and the diffraction peak broadening, associated to the X-ray grazing technique with a Curved position Sensitive detector. This analysis permits to follow different strain fields occurring during the phase transition.
- In the framework of the Landau–Ginzburg theory, we examine the $m \rightarrow t$ transition induced by irradiation and the $t \rightarrow m$ transition on isochronal annealing of irradiated samples in terms of dynamic effects of the order parameter induced by irradiation. This approach is quite different from the work of Levanyuk et al. [6], the so-called frozen defect approach, which analyses the impact of static defects (i.e. clusters) in the matrix on the phase transition.

2. Experiments and results

The chemical and crystallographic quality of samples analysed in this paper and the grazing X-ray instrument (Inel CPS-120) used to study effects of different irradiations have been detailed in a previous paper [1] and will not be described here.

2.1. Selection of different irradiations

In a previous paper [1], investigation of the zirconia phase transition induced by irradiation showed that the $m \rightarrow t$ phase transition induced by irradiation seems to occur in dense cascades. To confirm this point, four kinds of irradiations with different projectiles were performed:

- An irradiation by 1 MeV electrons until high dpa values (12 dpa) has been done at room temperature. Such an irradiation does not induce any cascades in the matrix. These results confirm previous results [1].
- An irradiation by O ions was performed. In this irradiation, cascades created along the oxygen path do not overlap. Oxygen projectiles with a kinetic energy of 400 keV were selected to reach large values of fluence.
- Two different irradiations by Xe and Bi ions have been done. These irradiations producing important overlappings of cascades along the projectile path

have been achieved at large fluence values to describe the kinetics of the $m \rightarrow t$ transition as a function of fluence. These irradiations were performed to investigate a possible saturation effect of the kinetic curve (cf. Fig. 4) as expected in our previous paper [1].

The kinetic energies of these ions have been chosen to produce path lengths sufficient to carry on grazing X-ray analysis above the critical angle [1]. The physical principle associated to the grazing X-ray is due to the fact that electrons are not free in solids. The existence of well-defined energy levels associated to chemical bonds leads to the existence of dispersion corrections [7]. These coefficients modifying the refractive index of the solid stop the penetration of X-rays into solids. This characteristic is used to probe the surface of materials by X-ray [8]. For CuKα1 radiation (used in this work), the kinetic energy of photons is equal to 8 keV. At this energy, photons interact only with core electron of the target. An irradiation, which does not transform the nuclei forming the target by nuclear reaction, leads to the apparition of extended (punctual) defects and phase transitions. These effects modify mainly the valence electron density of atoms in the neighbourhood of defects or of atoms participating in the phase transition. Then, the X-ray absorption coefficient (and then the critical angle) is not affected by irradiation.

The displacements per atoms (dpa) were calculated with displacement threshold energies of 20 eV for Zr and 60 eV for O atoms. Even if such values are somewhat arbitrary, all the dpa values can be directly compared. The number of dpa and the implantation profiles induced by Bi and Xe projectiles were calculated by TRIM-98 package (cf. Figs. 2(a) and (b)). We summarise in detail these different irradiations in Table 1. In the irradiation by electrons, the maximum energies transmitted by electrons to oxygen and zirconium atoms are, respectively, equal to 67 and 12 eV. These both values are superior to the threshold energy and must induce displacement in irradiated samples. No significant evolution of the reciprocal lattice was observed during this irradiation. This work confirms the previous analysis [1] that showed no phase transition of monoclinic ZrO_2 under electron irradiation even at high dpa values. The interest of a 400 keV O^+ irradiation is to create separated sub-cascades along the path of the projectile in the target. No phase transition was observed in these irradiated samples even at high dpa values. To exclude effects induced by the implantation peak in the 800 keV Bi^{2+} and 400 keV Xe irradiations, only 60 nm of ZrO_2 have been analysed by grazing X-ray diffraction. During these irradiations, an $m \rightarrow t$ phase transition is observed (cf. Table 1).

From the analysis of the kinetic curves of the $m \rightarrow t$ transition produced by these different kinds of irradiations, it is possible to analyse the impact of cascades overlapping on the phase transition. Figs. 2(a) and (b) present dpa, inelastic energy losses and implantation profiles due to 400 keV Xe and 800 keV Bi irradiations.

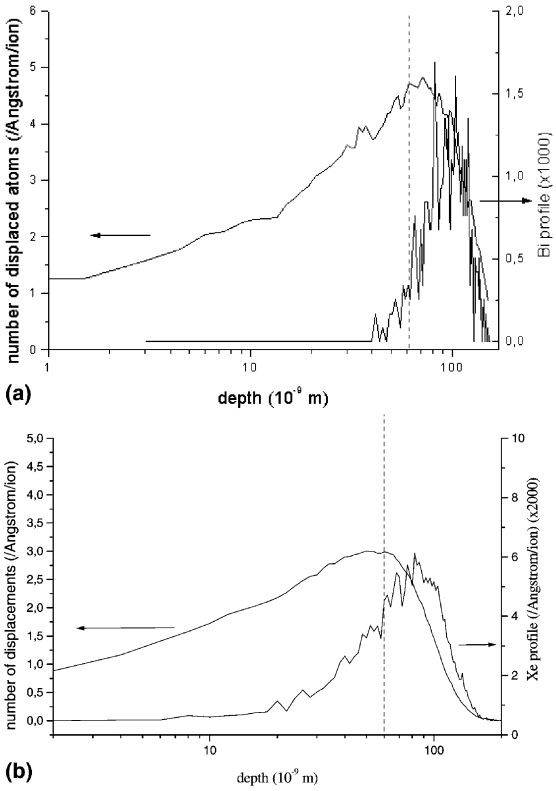

Fig. 2. Displacements per atoms and implantation peaks in ZrO_2 (5.83 g cm^{-3}) matrix computed with threshold energies are equal to 20 and 60 eV for Zr and O atoms. (a) Presents dpa and Bi implantation profiles due to 800 keV Bi irradiation, whereas (b) presents dpa and Xe implantation profiles due to 400 keV Xe irradiation. The vertical dash line is the limit of the area probed by X-ray (i.e. the thickness where 90% of the X-ray are diffracted by the material).

2.2. X-ray grazing diffraction analysis using the Rietveld method

This method induces a systematic shift of the incident angle in the solid and then leads to an overestimation of the Bragg angle and then of the lattice parameters. Moreover, a broadening of diffraction peaks is observed for incidence angles. This broadening mainly affects the gaussian components of the diffraction peaks. Errors on diffraction diagrams in grazing incidence on an Inel CPS 120 were studied in detail [9]. A Rietveld package, the XND program [10], has been modified to take into account these errors.

During refinements, different indicators define the quality of fits. Three of these indicators are presented in Table 2. R_{wp} is the quantity minimised during the

Table 1
Description of different irradiations performed on pure monoclinic zirconia samples

Nature and kinetic energy of projectiles	1 MeV electrons	400 keV O^+ ions	400 keV Xe^+ ions	800 keV Bi^{2+} ions
Temperature of irradiation (K)	300	300	300	300
Flux (cm^{-2} s^{-1})	1.1×10^{19}	1.1×10^{13}	1.1×10^{13}	1.1×10^{10}
Dpa	12	0.56–56	0.12–610	0.16–800
Displacement cross section (cm^{-2})	40×10^{-24}	5.8×10^{-16}	1.22×10^{-14}	1.60×10^{-14}
Atomic fraction of projectiles implanted in samples		2×10^{-4}–2×10^{-2}	2.6×10^{-5}–1.2×10^{-1}	1.9×10^{-5}–1.8×10^{-1}
Penetration length and straggling of projectiles		0.4 μm (0.09 μm)	0.085 μm (0.025 μm)	0.1 μm (0.03 μm)
Thickness probed by grazing X-ray (CuKα1)[a]		200 nm	60 nm	60 nm
Observed $m \rightarrow t$ phase transition	No	No	Yes	Yes

[a] 90% of the X-ray are diffracted in this thickness.

refinement. In our refinements; R_{wp} is calculated including the background contributions. The GofF is the ratio between a statistical estimation of the minimum R_{wp} obtainable for a given problem and R_{wp}. In our refinement, the GofF values are always superior to 1, indicating that errors on X-ray diagrams simulations are dominated by instrumental errors associated to the CPSD (all diagrams were overcollected). The GofF index is relatively insensitive to errors in the atomic structure model. The Bragg factor, R_B, is a measure of the agreement between the observed and calculated Bragg intensity and then characterises the structural model in the Rietveld refinements. All these indicators are listed in Table 2 for different refinements on irradiated samples.

To avoid effects induced by the implantation of Bi and Xe ions profile in ZrO_2, the incidence angles equal to 0.35° for Bi irradiations and 0.4° for Xe ions irradiations were chosen to analyse only 60 nm in the irradiated ZrO_2 samples. Fig. 3 presents the Rietveld analysis on ZrO_2 samples irradiated by 5×10^{16} Bi and Xe ions. Table 2 presents the evolution of unit cell parameters of two phases and the oxygen position in the tetragonal phase as a function of the fluence.

2.3. Experimental results

2.3.1. Measure of volume fractions associated to different phases

To describe the kinetics of the phase transition as a function of the fluences of different ions, the volume fraction of each phase has been obtained by measuring the integral intensity of the $2\theta_{-111}$ (28.17°) and $2\theta_{111}$ (31.5°) and $2\theta_{101}$ (30.17°) for the monoclinic and tetragonal phases. The calculated volume fractions computed by this method are in agreement with those obtained using scale factors in the Rietveld refinement. Fig. 4 presents the tetragonal volume fraction of ZrO_2 as

Table 2
Evolution of the different estimators qualifying the goodness of the Rietveld refinement (GofF), the quality of the structural model used in the refinement (R_B) and the quality of the data analysis (R_{wp})

Ions	Fluence (cm^{-2})	GofF	R_B^q	R_B^m	R_{wp}	a_t	c_t	a_m	b_m	c_m	β	Z_O
Bi	5×10^{16}	1.77	5.89	11.94	9.01	3.635(1)	5.189(3)	5.256(3)	5.317(3)	5.424(2)	99.2(1)	0.194(1)
Bi	10^{16}	1.71	4.68	11.30	8.07	3.625(0)	5.198(1)	5.201(9)	5.268(1)	5.314(8)	99.1(5)	0.205(1)
Bi	5×10^{15}	1.29	5.37	11.90	10.91	3.626(1)	5.170(3)	5.209(4)	5.260(6)	5.378(4)	99.1(4)	0.203(6)
Bi	10^{15}	1.30	4.39	11.34	11.00	3.626(1)	5.175(3)	5.210(4)	5.239(3)	5.374(4)	99.1(3)	0.202(1)
Bi	2×10^{14}	1.56	14.7	5.94	11.41	–	–	5.173(4)	5.224(1)	5.348(3)	99.1(4)	–
Bi	n.i.	1.29	–	3.06	10.89	–	–	5.182(4)	5.232(2)	5355(1)	99.1(0)	–
Xe	5×10^{16}	2.0	2.88	8.95	5.62	3.633(1)	5.178(4)	5.228(3)	5.247(3)	5.358(2)	99.2(1)	0.189(1)
Xe	10^{16}	1.70	3.12	8.96	9.31	3.630(1)	5.176(3)	5.198(4)	5.265(8)	5.369(2)	99.1(1)	0.205(3)
Xe	10^{15}	1.67	5.35	6.57	9.82	3.634(5)	5.174(2)	5.168(2)	5.219(2)	5.338(2)	99.1(1)	0.199(1)

The lattice parameters of the monoclinic and tetragonal phases are also presented as a function of dpa. The reduced oxygen position of the tetragonal phase is presented but the CuKα1 radiation and the diagram collection at room temperature do not permit to obtain accurate information on this data. The Debye Waller term is arbitrarily taken equal to 1 for both Zr and O atoms in all refinements.

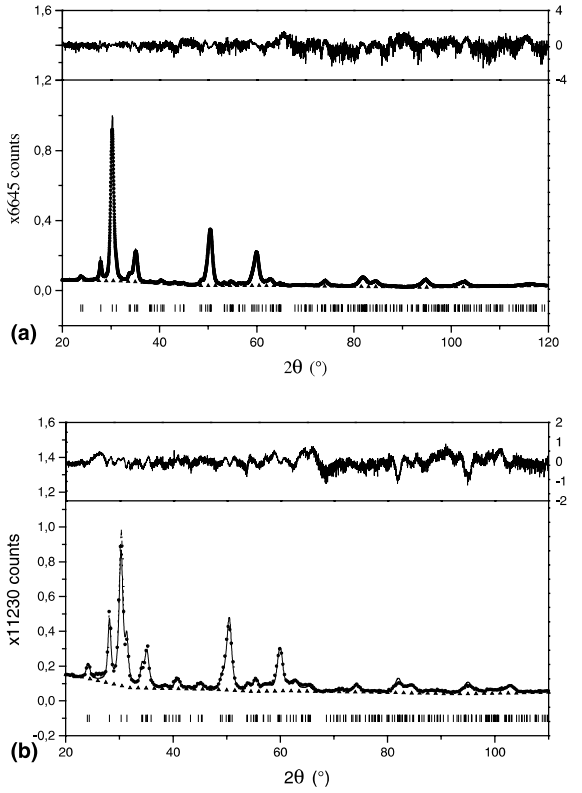

Fig. 3. Rietveld refinement on ZrO_2 samples irradiated by Bi ions with a kinetic energy of 800 keV at a fluence of 5×10^{16} ions with X-ray incidence angle of 0.35° (a) and by Xe ions with a kinetic energy of 400 keV at a fluence of 5×10^{16} ions with an incidence angle of 0.4° (b). Caption: black dots – collected X-ray diffraction diagram; black line – simulated X-ray diffraction diagram; up triangles – calculated background; black line near the top of the figure – fractional difference $(y_{exp} - y_{cal})/y_{exp}$ in each point divided by the standard deviation; black bars – Bragg peaks associated to the tetragonal and monoclinic phases.

a function of dpa for different irradiations by Bi and Xe ions at room temperature. Even at high dpa values, no variation of the X-ray background was observed for both Xe and Bi irradiations which means that no amorphisation has been recorded on these massive ZrO_2 samples. The X-ray diffraction diagram can only be fitted in space groups $P4_2/nmc$ and $P2_1/c$ for the tetragonal and monoclinic phases, respectively (Figs. 3(a) and (b)). There are no other phases. These results disagree with previous works [11] reported by Ossi [12].

2.3.2. Lattice parameters and macroscopic strain

The evolution of the unit cell parameters for both phases as a function of the fluence is presented in Table 1. No clear evolution of these parameters as a function of dpa can be presented. Moreover, the lattice parameters of the tetragonal phase produced by irradiation are

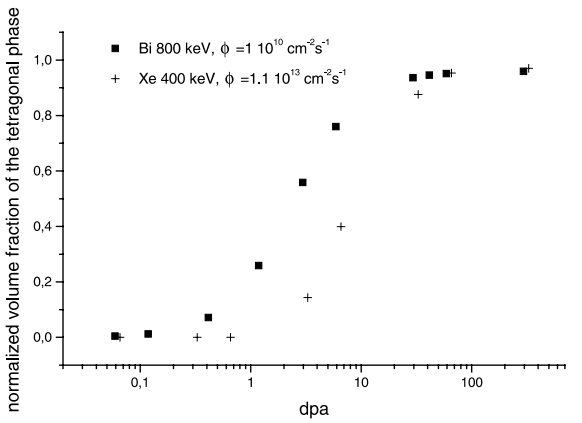

Fig. 4. Evolution of the volume fraction of the tetragonal ZrO_2 phase as a function of the dpa for 800 keV Bi irradiation (squares) and 400 keV Xe irradiation (circles).

not equal to those associated to the stabilised micrometric tetragonal phase or the nanometric tetragonal phase [9]. During the transition, both phases accommodated the variation of the volume induced by the phase transition ($V_t < V_m$). These results agree with the martensitic nature of the $m \rightarrow t$ transition. It can be shown that in such a transition, the long range strain is proportional to the total heterogeneous martensite volume [13]. The evolution of lattice parameters agrees with those obtained by neutron diffraction measurements [3].

2.3.3. Microscopic strain

The analysis of the broadening of monoclinic and tetragonal diffraction peaks permits us to estimate the local strain in each phase as a function of dpa for both irradiations. Figs. 5(a) and (b) present the evolution of the integral broadening as a function of the diffraction vector **s** [14]. Hall–Williamson curves drawn as a function of dpa for different irradiations do not possess non-null ordinate intercept. Only the slope, i.e. the local strain, of these curves increases as a function of dpa. The evolution of the local strain as a function of dpa is similar to that of the volume fraction of the tetragonal phase. This local strain may be understood as the excess of elastic energy associated to the interface wall of two phases or between different variants of the tetragonal phase coarsening during irradiation. As the tetragonal phase increases as a function of dpa, the interface wall and then the microstrains associated to the motion of this wall increase with dpa values.

Evolution of lattice parameters (Bragg angle positions) and local strain field (Hall–Williamson plots) is associated mainly to the $m \leftrightarrow t$ phase transition in zirconia. That is why it is very difficult to compare lattice parameters and local strain field measured on irradiated

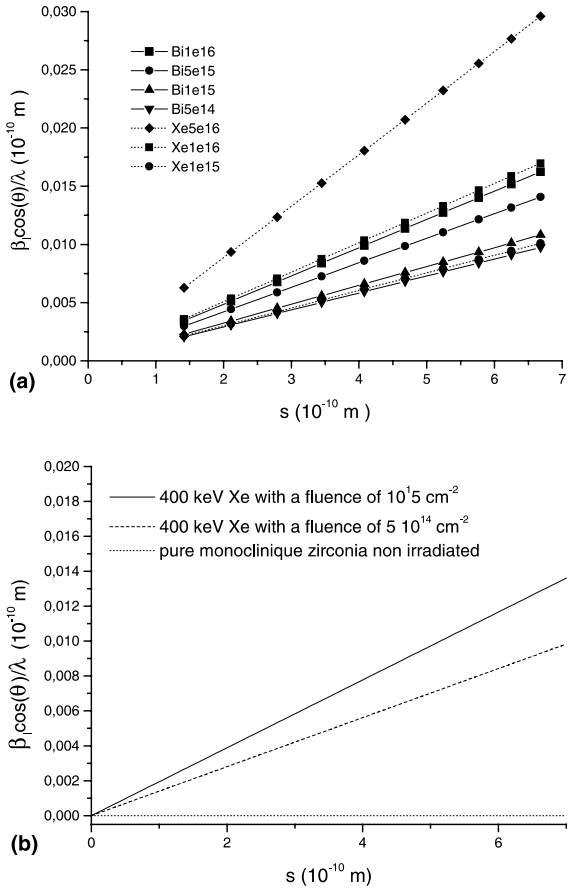

Fig. 5. Plot of the Hall–Williamson curves of the tetragonal (a) and monoclinic (b) phases for different Bi and Xe irradiations. During the Rietveld refinement, the evolution of the Lorentzian integral breadth part of the X-ray diffraction profile is fitted as a function of the Bragg angle to describe the broadening of Bragg peaks of different irradiated samples. The Hall–Williamson plots do not exhibit any evolution of the ordinate at the origin (no evolution of the CDD). Therefore, the evolution of the slope of the Hall–Williamson curves shows an increase of the local strain field both in the tetragonal and monoclinic phases. The local strain field reaches very crudely 4% in the tetragonal phase and 2% in the monoclinic phase.

samples to those measured on pure tetragonal phase (nanometric zirconia [9]). All Rietveld refinements were carried on with a free reduced atomic position of the oxygen atom in the tetragonal phase. Table 2 does not show a noticeable evolution of this parameter as a function of the fluence on irradiated samples. This is not surprising because X-ray diffraction is not a good probe to locate the oxygen position in ZrO_2 polycrystals. No clear comparison can be done between the atomic position on the tetragonal phase appearing under irradiation and the tetragonal phases existing in ZrO_2 nanopowders.

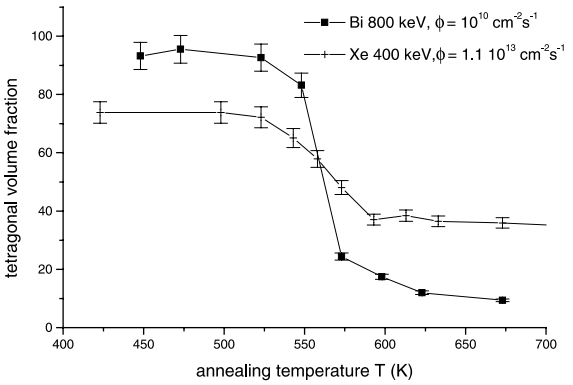

Fig. 6. Evolution of the tetragonal volume fraction as a function of the temperature for isochronal annealing of ZrO_2 samples irradiated by Bi 800 keV ions at a fluence of 10^{16} cm^{-2} and Xe 400 keV ion at a fluence of 5×10^{15} cm^{-2}. These curves clearly show the reverse $t \rightarrow m$ transition. The critical temperature is equal to 573 K.

2.3.4. Isochronal annealing of irradiated samples

To study the stability of the tetragonal phase induced by irradiation, different isochronal annealings (30 min) in air were done on a sample irradiated by Bi ions at a fluence of 5×10^{15} ions cm^{-2}. The annealing temperature range and the annealing time were chosen to avoid any diffusion of species in the irradiated samples ($T/T_m \leqslant 0.2$ with $T_m = 2973$ K for ZrO_2). Fig. 6 presents the overall kinetics of the reverse $t \rightarrow m$ transition. We observe a clear $t \rightarrow m$ transition during annealing out of irradiation. The temperature of the $t \rightarrow m$ phase transition (i.e. the critical temperature) was equal to about 573 K instead of 1073 K for the micrometric monoclinic zirconia powder. The large difference between the two critical temperature associated to the phase transition shows that the phase produced during irradiation is a metastable phase. The low value of this critical temperature under irradiation is too small to be associated to point defect diffusion, recombination or thermal dissolution of clusters induced by irradiation.

3. Discussion and modelling

All these experimental results give accurate information to present a possible model of the $m \rightarrow t$ phase transition under irradiation.

3.1. Effects of sub-cascades overlapping on the phase transition

During electron irradiations, no important displacement cascades are created. Under an irradiation by 400 keV oxygen projectiles, displacement sub-cascades do not overlap and no $m \rightarrow t$ transition appears. Following

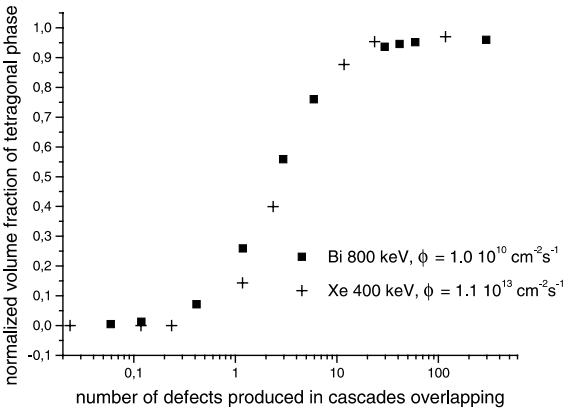

Fig. 7. 'Normalised' overall kinetic curve showing the evolution of the $m \rightarrow t$ phase transition as a function of the number of defects produced during the overlapping of sub-cascades for Xe and Bi irradiations.

these experimental results, it seems that the $m \rightarrow t$ transition is driven by the overlapping of sub-cascades. Following the work of Dettmann et al. [15], it is possible to calculate the overlapping of a cascade produced a $t = 0$ at a given point $\mathbf{r}$ in the matrix. We describe in detail the different points of our calculation in Appendix A. Following this formulation, it is possible to create a reduced scale for abscissa and to describe the phase transition induced by different ions by a unique curve (cf. Fig. 7). This normalised curve can be described by the following kinetic equation:

$$\frac{\mathrm{d}\theta}{\mathrm{d}\langle\mu\rangle} = k(1-\theta)\theta, \tag{1}$$

where k is a reaction kinetic constant, $\langle\mu\rangle$ is a function describing the effect of irradiation (cf. Appendix A) and θ is the normalised fraction of the tetragonal phase produced under irrradiation.

3.2. Mechanism of the phase transition

The clear group–subgroup relation between the tetragonal and monoclinic phases of zirconia leads us to suppose that this transition may be analysed in the Landau formalism [2]. In this framework, order parameters (i.e collective atomic motion of oxygen atoms in the case of zirconia) exist and the free energy of the system can be described in terms of these order parameters. Following the group theory formalism [2], the POP, called η in the following, can be understood as the shift of the oxygen atom, lying on the fourfold axis in the tetragonal phase. Following Negita and Takao [2], two primary order parameters (POP) associated to the motion of oxygen atoms (along the c-axis and in the plane perpendicular to the c-axis) can describe the transition (cf. Fig. 1). To obtain the correct strain field (controlling the c-axis tilt of the tetragonal phase) between two phases, one POP must trigger the motion of the two POPs, and then the analysis of the phase transition under irradiation consists in only to study the stability of this parameter under irradiation. We study the evolution of this parameter supposing that:

- either clusters produced at the end of displacement cascades modify the value of this parameter;
- or the sub-threshold energy laid down during the displacement cascades triggers the evolution of this parameter.

3.2.1. Cluster effect on the transition

We first suppose that clusters are created during the sub-cascade overlapping in the pure monoclinic zirconia. In fact, in the overlapping regions of different sub-cascades, the probability that point defects meet is maximum and the polymerisation of point defects to create extended defects, such as dislocation loops or clusters, can occur. These extended defects then generate an elastic strain field around them and modify the free energy phase diagram, making possible the $m \rightarrow t$ transition at room temperature.

If a periodic lattice of clusters exists in the irradiated area, the ordinate intercept of the Hall–Williamson plot associated to the tetragonal phase must vary. Such a variation is not observed (cf. Fig. 5(a)). Such results show either that no clusters are created in the irradiated material or that clusters are randomly created in the matrix by irradiation.

Following the work of Levanyuk et al. [6], these hypothetical clusters, randomly created in the matrix, can be considered as extended defects (frozen defects) produced by irradiation. These clusters modify the values of the POP describing the phase transition. Using the Landau–Ginzburg kinetic equation (cf. Appendix B), similar to the Cahn–Hilaire equation for diffusional processes, it is possible to compute the value of the POP considering that a cluster induces a small perturbation of the uniform POP in a domain defined by a correlation length ξ [16], and to calculate the defective free energy in this domain. If we suppose that defects act as independent defects, the defective free energy per defect can be written as

$$F_{\mathrm{d}} = F(\eta_0) + (f^{\mathrm{d}} - V_{\mathrm{d}} f(\eta_0)) + Ng2\pi r_{\mathrm{d}}(\eta_{\mathrm{d}} - \eta_0)^2 \times \left(1 + \frac{r_{\mathrm{d}}}{\xi}\right) \quad \text{and} \quad \xi^2 = \frac{g}{\alpha(T_{\mathrm{c}} - T)}, \tag{2}$$

where N is the density of defects produced during the irradiation, r_{d} is the radius of defect, η_0 is the uniform value of the POP, η_{d} is the value of the POP on the defect, T_{c} and T are, respectively, the critical temperature and the temperature at which the irradiated zirconia is analysed (i.e the isochronal temperature in our case), α

and g are described in detail in Appendix B. Then the excess of energy, for $r_d \ll \xi$, can be written as

$$W_d = N2\pi r_d(\eta_d - \eta_0)^2\left(1 + \frac{r_d}{\xi}\right), \tag{3}$$

W_d is a driving force allowing the phase transition.

The main part of the excess free energy is $W_d = N2\pi r_d(\eta_d - \eta_0)^2$, which does not vary with the temperature T.

During an isochronal annealing at a low temperature ($T/T_m = 0.2$), clusters produced under irradiation do not collapse and then the excess energy they induce does not vanish. This analysis disagrees with experimental results (cf. Fig. 6), which exhibits a $t \to m$ phase transition near 573 K for irradiated sample. Then it seems that clusters do not control the phase transition under irradiation.

3.2.2. Sub-threshold energy deposition

Now, if we focus our attention on displacement cascades, a part of projectile's energy is transferred to electrons of the lattice, the so-called inelastic stopping power. This energy is not sufficient to displace targets' nuclei far from their equilibrium positions. Therefore, it induces small displacement of the electric charges of unit cells carried by nuclei motions. The overlapping of cascades may allow by a cumulative effect the creation of a spontaneous polarisation over a large volume and a long time. An extra energy, W, must be added to describe the evolution of the POP evolution. The simplest form of W is

$$W = \mathbf{P}\cdot\mathbf{E} = \mathrm{Re}\, e\left(\frac{P^2}{\varepsilon_0(\varepsilon_r - 1)}\right) = \frac{e^2 z_{eq}^2 \nabla\eta^2}{\varepsilon_0(\mathrm{Re}\, e(\varepsilon_r) - 1)}, \tag{3a}$$

where $\mathbf{E}$ is the average electric field associated to $\mathbf{P}$, ε_0 and ε_r are respectively the dielectric and relative dielectric constants, z_{eq} is the equilibrium position of the oxygen atoms associated to the POP and e is the electron charge.

For a given volume recovering an important area the classical method for homogenisation of the spontaneous polarisation gives

$$\begin{aligned} W(r,t) &= \frac{1}{\tau_1}\int \frac{e^2 z_{eq}^2}{\varepsilon_0}\mathrm{Re}\, e\left(\frac{1}{\langle\varepsilon_r(r-r',t)\rangle - 1}\right)(\nabla\mathbf{n}(\mathbf{r}))^2\, \mathrm{d}^3\mathbf{r} \\ &= \frac{1}{\tau_1}\int f(r-r')(\nabla\mathbf{n}(\mathbf{r}))^2\, \mathrm{d}^3\mathbf{r}. \end{aligned} \tag{3b}$$

Following Pines [17], supposing that the medium can be approximated by an electron grazing which is a crude approximation in our case, the electronic stopping power in a jellium can be linked to the space and time Fourier transform of dielectric constant $\varepsilon_r(\mathbf{k},\omega)$ by

$$\frac{\mathrm{d}E_{st}}{\mathrm{d}z} \propto \int \omega\, \mathrm{d}\omega \int \mathrm{d}^3\mathbf{k}\, \mathrm{Im}\left(\frac{1}{\varepsilon_0\varepsilon_r(\mathbf{k},\omega)}\right)\delta(\omega - \mathbf{kv}), \tag{4a}$$

where $\mathbf{v}$ is the speed associated to the projectile.

In insulators with an important band gap like zirconia ($E_g \cong 6$ eV), Eq. (4a) is still valid [17].

Moreover, causality principle (i.e the Kramers Kronig relations) ensures a clear relation between the imaginary and real part of $\varepsilon_r(\mathbf{k},\omega)$ by

$$\mathrm{Re}\, e\left(\frac{1}{\varepsilon_r(\mathbf{k},\omega)} - 1\right) = \frac{1}{\pi}P\int \mathrm{Im}\left(\frac{1}{\varepsilon_r(\mathbf{k},\omega')}\right)\frac{\mathrm{d}\omega'}{\omega' - \omega}. \tag{4b}$$

The function $f(r,t)$ can be understood as the time-dependent density correlation function, which we suppose to be correctly described by a classical Ornstein–Zernike function $(1/r)\mathrm{e}^{-(r/\lambda)}$ (λ is a correlation length). The kinetic evolution of the POP, η, can be described by the following law:

$$\frac{\partial\eta}{\partial t} = -\frac{1}{\tau_2}\frac{\partial F}{\partial\eta} + \frac{\beta}{2}\int f(r-r')\nabla\eta(r')^2\, \mathrm{d}r', \tag{5}$$

where F is the Landau–Ginzburg free energy derived from the effective hamiltonian described in Appendix B.

The form of Eq. (5) does not allow a Lyapunov functional to be used to analyse the stability of the phase as it can be done under irradiation for ordered material [19]. We study the phase stability of the system by a local analysis. Near the equilibrium value of the POP, η_e, describing the monoclinic phase, we focus our attention on the fluctuation of η, $\delta\eta$. The evolution of the Fourier transform $\delta\eta(\mathbf{k},t)$ of $\delta\eta(\mathbf{r},t)$ is governed by the following linearised equation (cf. Appendix C introducing the reduced time scale $x = t/\tau_1$):

$$\frac{\partial\delta\eta(k,x)}{\partial x} = -\frac{\tau_1}{\tau_2}(L'' + gk^2) + \beta f(k)k^2, \tag{6a}$$

τ_1/τ_2 is a factor describing the coupling between the irradiation and the material response. For $\tau_1/\tau_2 \gg 1$, irradiation acts like a shock wave. For τ_1/τ_2 near unity, irradiation drives the behaviour of the material, allowing it to explore the space phase. We now suppose that this latter condition is fulfilled. Expecting a relaxation mechanism of the fluctuation exponential, $\delta\eta(k,t) = \delta\eta(k,0)\mathrm{e}^{-\omega(k)t}$, we obtain, introducing the scale factor τ_1/τ_2 in the first expression of Eq. (6a):

$$\begin{aligned} \omega(k) &= L'' + gk^2 - \beta f(k)k^2 \\ &= \beta\left(\frac{L''}{\beta} + \frac{g}{\lambda^2\beta}k^2\lambda^2 - \frac{\lambda^2k^2}{1+\lambda^2k^2}\right) \\ &= \beta\left(\gamma(T_c - T) + \frac{g}{\lambda^2\beta}k^2\lambda^2 - \frac{\lambda^2k^2}{1+\lambda^2k^2}\right). \end{aligned} \tag{6b}$$

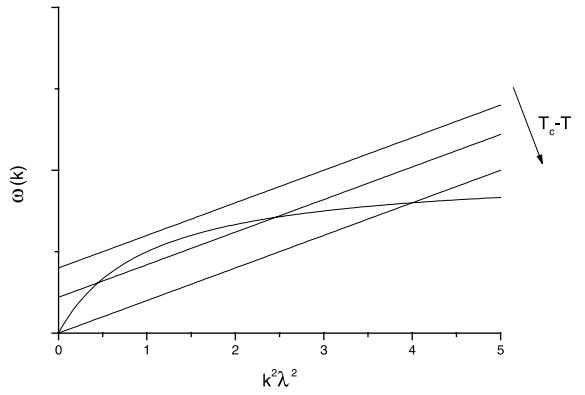

Fig. 8. Comparison of analytical functions used to compute the amplification factor associated to POPS' fluctuations as a function of the wave vector **k** for a given temperature. Some area exists in the (k,ω) plane in which $\omega(k)$ becomes negative. Caption: Different linear curves possess a unique slope equal to 0.1 and intercepts at the ordinate equal to 0, 0.2 and 0.4, respectively.

The stability of the monoclinic phase in a classical phase diagram imposes that $L'' = \partial^2 L/\partial\eta^2 > 0$, (i.e. any fluctuation is damped). Under irradiation, there exist some areas in the $(\lambda^2 k^2, \omega)$ plane in which some fluctuations are amplified leading to the propagation of instabilities and then triggering the phase transition (cf. Fig. 8). Replacing L (in Eq. (6b)) by a linear function of the temperature as it is usually the case in the Landau theory, the effect of the temperature under irradiation on the phase transition can be investigated.

In this framework, experimental results can be understood:

- The function μ, used to describe the overall kinetic transition described in detail in Appendix A, is roughly proportional to the sub-threshold energy deposited by cascades overlapping in the area probed by X-rays.
- As the transition is driven by energy laid down by displacement cascades, the volume fraction of the tetragonal phase is noticeable only in areas where the inelastic energy loss is important, i.e. the area where the damage profile is important. This analysis explains the experimental results describing the presence of the tetragonal phase as a function of the X-ray probed depth for a given irradiation at fixed dpa value [1].
- The amplification of fluctuations under irradiation allows the system to reach a non-global minimum describing the tetragonal phase. This 'metastable state' is no more associated to static defects produced by irradiation. Out of irradiation, isochronal annealings give enough energy to the system to pass through the energy barrier associated to this state. The height of the kinetic barrier depends on the form of the 'pseudo' free energy under irradiation and this form is not similar to the form observed out of irradiation. That is why the critical temperature measured on annealed irradiated samples is not linked to the critical temperature of the system out of irradiation.
- If we suppose that the evolution of the POP far from equilibrium is the limiting step of the transition, the kinetics of the transition can be understood. Following the Ornstein–Zirnike formalism [18], the X-ray diffracted intensity is linked to the time-dependent pair correlation function by

$$\begin{aligned} I(k,t) &\propto \int G(r,t)\mathrm{e}^{\mathrm{i}kr}\,\mathrm{d}r \\ &= \int \langle(\delta(r - R_j(0)))(\delta(r + r' - R_j(t)))\rangle \mathrm{e}^{\mathrm{i}kr}\,\mathrm{d}r \\ &= \int \langle(\delta\eta(r,0))\delta\eta(r + r',t)\rangle \mathrm{e}^{\mathrm{i}kr}\,\mathrm{d}r, \\ I(k,t) &\propto \langle\delta\eta(k,0)\delta\eta(k,t)\rangle = \langle\delta\eta(k,0)\rangle \mathrm{e}^{\omega(k)x} \end{aligned} \tag{7}$$

The volume fraction of the tetragonal phase is proportional to the (1 0 1) tetragonal peak. Then the kinetic equation (Eq. (1)) is nothing else than Eq. (7). The form of the kinetic equation can now be understood. For low μ values, the overlapping of cascades is not sufficient to generate an important shock wave (i.e. $\tau_1/\tau_2 \gg 1$). For medium μ values, Eqs. (6a), (6b) describe the evolution of the system, and the logarithm of the volume fraction of the tetragonal phase varies linearly as a function of μ (i.e. x). For high μ values, the growth of tetragonal phases is limited by short range strain fields associated to their interfacial walls.

- Under irradiation by swift heavy ions, experimental results summarised in a recent paper [20] clearly exhibit an $m \to t$ transition in zirconia. Replacing the source term, associated to the sub-threshold energy deposition in cascades, driving the POP evolution by the shock wave generated along the projectile path [21], it is possible to describe the evolution of the POP in the same way. The kinetic equation is no longer described by cascade overlapping but by the stopping power, related to the extra electric field, of the incident projectile.

4. Conclusion

This work extends previous studies of zirconia behaviour under irradiation using the grazing X-ray analysis. From the Rietveld analysis, it is possible to obtain valuable information on the kinetics of the $m \to t$ phase transition driven by irradiation and on the distortions of unit cells induced by the transition. The use of Rietveld analysis clearly shows that no amorphisation has been detected on irradiated samples by Bi and Xe

ions. The X-ray diffraction diagram can only be fitted in space groups $P4_2/nmc$ and $P2_1/c$ for the tetragonal and monoclinic phases, respectively. Short range strain field is clearly observed and correlated to the martensitic nature of the transition. The evolution of unit cell parameters during irradiation may be understood as the accommodation of crystallographic misfits of two phases classically observed in a martensitic transition. For different incident projectiles, overall kinetics describing the $m \rightarrow t$ transition were plotted. The analysis of these overall kinetics clearly permits us to show the importance of cascades overlapping in the transition mechanism. As a clear group–subgroup relation exists between the tetragonal and monoclinic phase of zirconia out of irradiation, the notion of primary order parameter triggering the transition, developed by Landau, was used to describe the phase transition. Introducing a source term due to irradiation by energetic projectiles, it is possible to explain the observed transition under irradiation by the amplification of POPs' fluctuations. The above model is characterised by a cumulative transfer of energy laid down in displacement cascades. This transfer is coherent in space and time. In this framework, the evolution of the overall kinetics of the transition during annealing out of irradiation can be clearly understood.

Therefore, two main problems are associated to this model:

- The first one comes from the fact that the $m \rightarrow t$ transition out of irradiation is not clearly understood. Some experiments are carried on in our laboratory to follow the evolution of POP as a function of the temperature, and to confirm that the zirconia $m \leftrightarrow t$ phase transition can be understood in the Landau framework.
- The second one is due to the fact that the model is based on phenomenological coefficients which may be difficult to measure. As irradiations by energetic ions (GANIL experiments) do not present displacement cascades, such an irradiation may give valuable information on the phenomenological coefficient, the β term, describing the coupling between the POP gradient and the 'irradiation force'.

We carry on investigation in our laboratory to confirm these two points.

Acknowledgements

We acknowledge Professor C. Lemaignan for the interesting discussions on zirconia phase transition, Dr P. Dubuisson and I. Monnet for the irradiation by 1 MeV electrons and TEM observations of zirconia samples and M. Plantier for irradiation of zirconia samples by O, Xe and Bi ions.

Appendix A

If we suppose that a defined sub-cascade is created in a box with a characteristic length L at $t = 0$, it is necessary to calculate the probability that other cascades be created in the same box during a time t. The first step of the calculation is to compute the probability that different sub-cascades occur in the box. In other words, the mean free path of sub-cascade creation must be estimated. Let N be the number of atoms per unit volume in the crystal, and the probability is

$$P_1(t) = LN\sigma^{\mathrm{p}} = LN \int_{E_{\mathrm{c}}}^{\mu E} \frac{\mathrm{d}\sigma}{\mathrm{d}T}\,\mathrm{d}T \approx LN \int_{E_{\mathrm{d}}}^{\mu E} \frac{\mathrm{d}\sigma}{\mathrm{d}T}\,\mathrm{d}T,$$

where σ^{p} is the primary displacement cross-section, E_{c} is the energy below which a sub-cascade is created, E_{d} is the threshold energy in the material, μ is a kinematic factor describing the maximum energy transmitted to a PKA and $\mathrm{d}\sigma/\mathrm{d}T$ is the differential cross-section describing the collision between the projectile and the PKA. The generalisation of this formula to polyatomic materials is straightforward.

The next point of the calculation is to compute the overlapping of sub-cascades in the box. In the volume, L/ϕ per time unit, the number of sub-cascades created is $((\sigma^{\mathrm{d}}/\sigma^{\mathrm{p}}) - 1)$, where σ^{d} is the total displacement cross section. Associating the volume of each sub-cascades to Ω, it is possible to define a characteristic time of sub-cascade overlapping occurrence τ by

$$\tau = \frac{L}{\phi}\,\frac{1}{2\Omega((\sigma^{\mathrm{d}}/\sigma^{\mathrm{p}}) - 1)}.$$

The probability to obtain an overlapping of k sub-cascades is $P_k(t) = (t/\tau)^k(1/k!)\mathrm{e}^{-t/\tau}$. Then, the probability that more than one sub-cascade be produced in the box L is $(1 - P_0(t))$. Hence the probability of cascades overlapping is

$$P(t) \approx P_1(t)P_2(t) = NL\sigma^{\mathrm{p}}\left(1 - \mathrm{e}^{-t/\tau}\right).$$

As the profile of the sub-threshold energy laid down in the matrix is proportional to the dpa profile (cf. Figs. 2(a) and (b)), the total sub-threshold energy deposed is proportional to $\mu = P(t) \cdot \mathrm{dpa}$.

For an irradiation by electrons, $\sigma^{\mathrm{d}} = \sigma^{\mathrm{p}}(1 + \varepsilon)$, where $\varepsilon \ll 1$ and $\mu_{e^-} = NL\sigma^{\mathrm{p}}\varepsilon t$, which is smaller than unity.

For an irradiation by O^+ ions, the primary displacement cross-section, σ^{p}, is two orders of magnitude smaller than for Xe and Bi ions, which means that the characteristic mean free path between two sub-cascades is high and the probability that a sub-cascade overlapping occurs, is small.

Using numerical values both for Xe and Bi ions, it is possible to compute the average value of the energy laid

down by the displacement cascade overlapping. For sub-cascades radii equal to 10 nm, a characteristic length L equal to 60 nm (simulation of TRIM-98) and fluxes equal to 1.1×10^{-3} and 1×10^{-6} Å^{-2} s^{-1} (cf. Table 1), the average of μ, $\langle\mu\rangle$ can be written as

$$\langle\mu\rangle = NL\sigma^{\text{p}}\frac{1-\tau}{\tau}\ \text{dpa} \approx NL\sigma^{\text{p}}\frac{1}{\tau}\ \text{dpa}.$$

Such a formulation has been used to define the normalised kinetic equation of Fig. 6.

The probability density associated to $p(t)$ can be written as

$$p(t) \approx \frac{NL\sigma^{\text{p}}}{\tau}\text{e}^{-t/\tau}.$$

The mean value of a function $f(r,t)$ during the cascades overlapping is then

$$\langle f\rangle = \int f(r,t)p(t-t')\,\text{d}t' = \frac{f(r)}{\tau}.$$

Appendix B

In a defective system, defects modify the value of the POP. These so-called frozen defects lead to an inhomogeneous system where the Landau free energy is then described by the Landau–Ginzburg effective hamiltonian. This hamiltonian, analogous to the Cahn–Hilaire equation for diffusional processes, is written as

$$H_{\text{eff}}(\eta) = L(\eta) + \frac{g}{2}(\nabla\eta)^2,$$

where L is the classical Landau hamiltonian, g is a positive phenomenological coefficient and ∇ is the gradient operator induced by defects in the volume. This hamiltonian describes non-local inhomogeneities in the defective system.

Considering non-interacting spherical defects, the Landau–Ginzburg free energy can be described by

$$F(\eta(\mathbf{r})) = f_{\text{d}} + \int_{V-V_{\text{d}}} H_{\text{eff}}(\eta(\mathbf{r}))\,\text{d}V,$$

where f_{d} is the free energy associated to extended defects of volume V_{d}.

Minimisation of this functional with respect to $\eta(\mathbf{r})$ leads to

$$g\Delta\eta = \frac{\partial L}{\partial\eta},$$

$$\eta(r_{\text{d}}) = \eta_{\text{d}},$$

$$\eta(\infty) = \eta_0,$$

where r_{d} is the radius of the defect, η_{d} is the value of POP at the surface of the defect and η_0 is the POP value of the undisturbed system.

Supposing that the perturbation remains small compared to η_0, and taking into account only the first term of the Landau free energy, it is possible to compute the function $\eta(\mathbf{r})$ by

$$\eta(r) = \eta_0 + (\eta_{\text{d}} - \eta_0)\frac{r_{\text{d}}}{r}\text{e}^{-(r-r_{\text{d}})/\xi}$$

and

$$\xi^2 = \frac{g}{(\partial^2 L/\partial^2\eta)} = \frac{g}{\alpha(T_{\text{c}} - T)},$$

where $\alpha(T_{\text{c}} - T)$ is the classical form of phenomenological coefficient associated to the fourth-order term of the Landau free energy.

$\eta(\mathbf{r})$ is analogous to the Ornstein–Zernike function and ξ can be understood as a correlation length above which no noticeable effect of the defect on the POP can occur. We have taken into account only the first term of the Landau free energy, which depends classically on the difference between the critical temperature and the temperature at which the irradiated zirconia is analysed. The free energy of the defective system is now

$$F^{\text{d}} \approx f_{\text{d}} + (V - V_{\text{d}})f(\eta_0) + 2\pi g r_{\text{d}}(\eta_{\text{d}} - \eta_0)^2\left(1 + \frac{r_{\text{d}}}{\xi}\right).$$

Then the extra energy between the unperturbed and defective system can be expressed as

$$\begin{aligned}\Delta Fd &\approx (f_{\text{d}} - V_{\text{d}}F(\eta_0)) + 2\pi g r_{\text{d}}(\eta_{\text{d}} - \eta_0)^2\left(1 + \frac{r_{\text{d}}}{\xi}\right)\\ &\approx 2\pi g r_{\text{d}}(\eta_{\text{d}} - \eta_0)^2\left(1 + \frac{r_{\text{d}}}{\xi}\right)\\ &= W_{\text{d}}.\end{aligned}$$

We have neglected the excess free energy of the defect because its volume is small compared to the correlation volume ξ^3.

Appendix C

The simplest way to form an energy with $f(r)$ and the order parameter is to suppose a coupling of the form $f(r)\nabla\eta^2(r)$. Then the energy describing the evolution of the POP under irradiation can be written as

$$F = \int L(\eta) + \frac{g}{2}(\nabla\eta)^2\,\text{d}V + \frac{\beta}{2}\int f(r-r')(\nabla\eta)^2\,\text{d}V,$$

where β is the coupling coefficient. This coefficient is supposed to be positive in order to ensure that the equilibrium phase out of irradiation is the most stable state. Supposing that out of the domain V, the order parameter does not evolve, it is possible to compute the

first variation of F as a function of the perturbation $\delta\eta(r,t)$. We obtain

$$\delta F = \int \frac{\partial L}{\partial \eta} + g\nabla\eta\nabla\delta\eta \, \mathrm{d}V - \beta \int f(r-r')\nabla\eta\nabla\delta\eta \, \mathrm{d}V.$$

As $\delta\eta(r,t)$ is equal to zero at the boundary of the domain, we obtain

$$\delta F = \int \frac{\partial L}{\partial \eta} - g\Delta\eta\delta\eta \, \mathrm{d}V + \beta \int f(r-r')\Delta\eta\delta\eta \, \mathrm{d}V,$$

η describes a stable equilibrium point, the first derivative of L is null and the second derivative of L must be positive. Then the first variation of F is

$$\frac{\delta F}{\delta \eta} = \int \left(\frac{\partial^2 L}{\partial \eta^2} - g\Delta\eta \right) \mathrm{d}V + \beta \int f(r-r')\Delta\eta \, \mathrm{d}V.$$

References

[1] D. Simeone, J.L. Bechade, D. Gosset, A. Chevarier, P. Daniel, H. Pilliaire, G. Baldinozzi, J. Nucl. Mater. 281 (2000) 171.

[2] K. Negita, H. Takao, J. Phys. Chem. Solid 50 (3) (1989) 325.

[3] H. Boysen, F. Frey, T. Vogt, Acta Crystallogr. B 47 (1991) 881.

[4] E. Kisi, C. Howard, in: Key Engineering Materials, vol. 1, Trans Tech, 1998, p. 153.

[5] O. Blashko, V. Dimitriev, G. Krexner, P. Toledano, Phys. Rev. B 59 (14) (1999) 9095.

[6] A. Levanyuk, V. Osipov, A. Sigov, A. Sobyanin, Sov. Phys. JETP 49 (1979) 176.

[7] H. Wgenfeld, Theoretical Computation of X-ray Dispersion Correction, Copenhagen, 1975, p. 13.

[8] M. Brunel, F. De Bergevin, Acta Crystallogr. A 42 (1986) 299.

[9] P. Bouvier, E. Djurado, G. Lucazeau, T. Le Bihan, Phys. Rev. B 62 (13) (2000) 8731.

[10] J.F. Berar, G. Baldinozzi, CPD Newsletter 20 (1998) 3.

[11] A.R. Gonzalez-Elipe, F. Yubero, J.P. Esponos, A. Caballero, M. Oscana, J.P. Holgado, J. Morales, Surf. Coat. Technol. 125 (2000) 116.

[12] P.M. Ossi, J. Nucl. Mater. 289 (2000) 80.

[13] A. Khachaturyan, Theory of Structural Transformation in Solids, Wiley, New York, 1983.

[14] A. Klug, X-ray Diffraction Procedure, Wiley, New York, 1966.

[15] K. Dettmann, G. Liebfried, K. Schroeder, Phys. Stat. Sol. 22 (1967) 433.

[16] E. Stanley, Phase Transition and Critical Phenomena, Oxford University, Oxford, 1971.

[17] D. Pines, Elementary Excitations in Solids, Benjamin, New York, 1963.

[18] E. Salje, Phase Transition in Ferro Elastic and Co Elastic Crystals, Cambridge University, Cambridge, 1993.

[19] G. Martin, Phys. Rev. B 30 (3) (1984) 1424.

[20] C. Gibert-Mougel, F. Couvreur, J.M. Costantini, S. Bouffard, F. Levesque, S. Hemon, E. Paumier, C. Dufour, J. Nucl. Mater. 295 (2001) 121.

[21] D. Lesueur, A. Dunlop, Radiat. Eff. Def. Solids 126 (1993) 163.